THE ASTROPHYSICAL JOURNAL, 293:356–369, 1985 June 15

THE MULTIPLE IMAGES OF THE QUASAR 0957+561

D. H. ROBERTS,[1] P. E. GREENFIELD,[2,3] J. N. HEWITT,[2] B. F. BURKE,[2] AND A. K. DUPREE[4]
Received 1984 August 6; accepted 1984 December 29

ABSTRACT

The gravitationally imaged double quasar 0957+561 has been observed at an angular resolution of 0".3 using the full VLA at 6 cm wavelength. The radio source G (2.3 mJy) was clearly resolved (deconvolved size 0".33 × 0".14 at P.A. = 166°); its centroid lies slightly north of both the nucleus of the primary lens galaxy G1 and the third VLBI component G′. Thus most of the flux in G is probably intrinsic to G1; its radio properties are quite similar to those of M87. Although the flux and position of G are consistent with the hypothesis that G′ is the third quasar image B2, models fitted to the VLA structure of G do not include the anticipated point component. Limits on the flux of B2 as a function of its separation from the nucleus of the lens galaxy G1 are presented. Comparison of the maps with models of the imaging process suggests that the third quasar image lies within 0".2 of the nucleus of the primary lens galaxy G1 and contains less than 1% of the flux of the bright B image. The possibility that 0957+561 is quintuple, and that the sum of the three missing images is the G radio source, is considered and found to be compatible with the optical and radio data if the three aditional optical images suffer 1.6 mag of extinction in passing through the nucleus of the lens galaxy G1.

A weak new radio source "BN," with flux 0.34 mJy, was discovered 0".35 north of the bright B quasar image. Detailed models of the image formation, compatible with previous radio and optical observations, predicted that the VLA radio jet, whose first image extends northeast of quasar image A, should have a second image of 0.4 mJy lying between the bright B quasar image and the nucleus of G1. This is the most likely explanation of BN, since it is very difficult to produce a third quasar image which is as close to B as is BN and yet contains only about 1.4% of B's flux.

Subject headings: interferometry — quasars — radio sources: galaxies — relativity

I. INTRODUCTION

There is overwhelming evidence that the twin quasar 0957+561 is an example of gravitational lensing (Walsh, Carswell, and Weymann 1979; Young *et al.* 1980, 1981; Greenfield, Burke, and Roberts 1980). The two quasar images exhibit essentially identical optical spectra (Walsh, Carswell, and Weymann 1979; Weymann *et al.* 1979; Wills and Wills 1980), and there is a foreground galaxy (the "primary lens galaxy" G1, about 1" north of the B quasar) of sufficient mass to produce the 6" separation of the A and B quasar components (Young *et al.* 1980; Stockton 1980). Radio observations at arc second resolution show compact radio counterparts of the optical images, as well as an arc second jet and extended emission associated with the A quasar (Pooley *et al.* 1979; Roberts, Greenfield, and Burk 1979; Greenfield, Roberts, and Burke 1980; Greenfield, Burke and Roberts 1980; Noble and Walsh 1980). Very long baseline interferometry has shown that both A and B possess the core-jet morphology typical of many quasars (Porcas *et al.* 1979, 1981; Haschick *et al.* 1981; Gorenstein *et al.* 1980, 1983).

Models of the imaging process which attempt to account for the detailed configuration of optical and radio images require the presence of a substantial quantity of unseen matter in the cluster in which the foreground galaxy is located (Young *et al.* 1980, 1981; Greenfield 1981; Greenfield, Roberts, and Burke 1985). A gravitational lens consisting of a mass distribution which is free of density singularities must produce an odd number of images of each object lying behind it (Bourassa and Kantowski 1975; Dyer and Roeder 1980; Young *et al.* 1980; Burke 1981). An important unsettled problem in 0957+561 is thus location of the as yet unidentified third quasar image. According to models of the imaging process in 0957+561, the bright southern quasar component B (the "B1" image) must be accompanied by a "B2" image which lies somewhere between the bright B component and the nucleus of the primary lens galaxy G1. The VLBI measurements have shown that the B2 image does not lie very close (a few milli-arcsec [mas]) to the B1 image, but Gorenstein *et al.* (1983) have reported the discovery of a third VLBI component, which they call G′, lying close to the nucleus of the galaxy G1; this could be the third quasar image. Stockton (1980) has placed a limit on the total optical intensity of any quasar images near the lens galaxy G1 of 2% of the brightness of the B quasar image. Refsdal (1964) pointed out that relative time delay measurements in gravitational lenses could be used to measure cosmological parameters such as Hubble's constant, and Young *et al.* (1981) showed how the third image can be particularly useful in so doing in this complicated system. Furthermore, any detailed lens model must be compatible with the location and intensity of the third quasar image (or limits thereon).

An extensive series of multiband radio observations of 0957+561 made with the Very Large Array (VLA) of the NRAO[5] are presented by Greenfield, Roberts, and Burke (1985). In the present paper the highest quality data from that series are combined with a new set of high-resolution observations made at 6 cm wavelength using the full VLA. These observations demonstrate structure in the B radio quasar com-

[1] Brandeis University.
[2] Massachusetts Institute of Technology.
[3] Bell Telephone Laboratories.
[4] Harvard-Smithsonian Center for Astrophysics.

[5] The National Radio Astronomy Observatory is operated by Associated Universities, Inc., under contract from the National Science Foundation.

ponent and in the radio source G which lies close to the nucleus of primary lens galaxy G1. When combined with the optical data of Stockton (1980) and the recent VLBI data of Porcas *et al.* (1981) and Gorenstein *et al.* (1983), our data show that most of the flux in the G radio source is probably due to a nuclear source intrinsic to the lens galaxy G1. The radio properties of this galaxy are similar to those of M87. The structure of the B quasar region is consistent with the predictions of Greenfield (1981), strongly suggesting that an additional image of the arc second radio jet has been found. No unambiguous evidence for the third quasar image B2 was found near B or near the galaxy G1, but limits are obtained on the intensity of B2 as a function of its separation from the nucleus of the lens galaxy G1.

II. MODELS FOR THE FORMATION OF THE 0957+561 IMAGES

Studies of the gravitational lensing in 0957+561, using King mass distributions for the galaxy G1 and for the rich cluster which surrounds it, have been made by two groups (Young *et al.* 1980, 1981; Greenfield 1981; Greenfield, Roberts, and Burke 1985). These models include parameters for the shape, location, and velocity dispersion of the lensing matter and for the position and configuration of the object quasar. With so many degrees of freedom one might expect that several sets of parameters could be found which would satisfy the observations; however, both groups of authors found that this was not the case. Young *et al.* (1981) commented that fitting the observed image morphology "strained the capacity of the ... models." Greenfield added the relative orientations of the VLBI structures of A and B to the constraints and found it even more difficult to find any model which reproduced the configurations and brightness observed on all angular scales. In the best model (his "Model 2"; see Greenfield, Roberts, and Burke 1985), the observed core-jet position angle of 21° at A corresponded to a position angle of 5° at B, while the data of Porcas *et al.* (1981) gave 17° at B. The discrepancy is probably not serious, however, as Gorenstein and Rogers (1982) have indicated that the two-component Gaussian models used by Porcas *et al.* are too limited to account for the actual structure of the VLBI sources. Thus in what follows we will use the gravitational lens models of Greenfield, Roberts, and Burke as a guide to the interpretation of the new features which appear in 0957+561 at the resolution and dynamic range of the maps presented below.

III. OBSERVATIONS AND DATA REDUCTION

The source 0957+561 was observed with the VLA in its largest configuration (A array) at 6 and 18 cm wavelength (4885.1 and 1635.1 MHz respectively) over a period of 12 hr on 1980 December 16, and at 6 cm for 5 hr on 1982 May 8. Each data set was calibrated in phase with the nearby point source 1031+567, and the fringe amplitudes were referred to 3C 286, taking into account the slight resolution of this source with the longer VLA baselines (Perley 1982; Greenfield, Roberts, and Burke 1985). The standard DEC-10 calibration programs and AIPS map-making routines of the NRAO were used in the data reduction.

Each edited and calibrated data set was (separately) made into a uniformly weighted "dirty" map of 512 × 512 cells each 0″.075 square. These were CLEANed using the algorithm of Clark (1980), and the resulting maps, which had measured rms noise levels of 75–80 μJy per beam area, were used as input models for the self-calibration routine ASCAL (Schwab 1980, 1981). This procedure determines time-dependent corrections to the amplitude and phase gains of each of the antennas in the array by minimizing the weighted mean-square difference between the data and a model source visibility. The gain corrections are then applied to the data, and the resulting corrected visibilities processed into a new map. For each data set this self-calibration procedure was iterated four times. The first two passes permitted phase-gain corrections only and used a relatively small number of clean components (a few hundred) to generate the model visibility. The last two passes also permitted amplitude-gain corrections, initially against a model visibility derived from a few hundred components, and finally against all 12,000–16,000 components which were needed to adequately clean the maps (with a loop gain of 0.1). In all cases only those visibilities on baselines greater than 100,000 wavelengths were used to derive the gain corrections. The procedure was terminated because the last iteration yielded no significant change in the map. The noise levels of the final maps (denoted 80DEC1 and 82MAY1) are given in Table 1, where they may be seen to range from 30 to 42 μJy per beam, about 1.4 times the anticipated thermal noise calculated from the on-source time and nominal equipment parameters for the VLA, assuming that each visibility point has equal weight.

In order to compensate for the preponderence of short interferometer spacings typical with the VLA, the AIPS parameter UVBOX, which determines the size of the region in the *u-v* plane used to derive the weight of a visibility point at its center, was allowed to take several values between one (canonical "uniform weighting," used above) and eight. The effect of this "super uniform weighting" procedure is to weight the longer baselines more heavily, resulting in resolution closer to that of a completely filled aperture (Sramek 1982). It was found that the choice UVBOX = 4 was optimal, enhancing resolution

TABLE 1

PARAMETERS OF 6 cm VLA MAPS OF THE DOUBLE QUASAR 0957 + 561

Epoch	Map Name	UVBOX	Time (hr)	Clean Beam	rms Noise (μJy) Measured	rms Noise (μJy) Calculated
1980 Dec 16	80DEC1	1	2.88	0″.40 × 0″.35 @ 120°	37	25
1980 Dec 16	80DEC4	4	2.88	0.29 × 0.27 @ 118°	30	25
1982 May 8	82MAY1	1	2.50	0.36 × 0.30 @ 167°	42	27
1982 May 8	82MAY4	4	2.50	0.27 × 0.25 @ 161°	33	27

NOTE.—The parameter UVBOX determines size of the box used to derive the weight for a given *u-v* cell at its center. Observing time is the time in which a full 27 antenna array would gather the number of visibility points in the data. The measured noise level is the average from three apparently empty sections of the map field within 10″ of the source; the calculated noise, determined from the observing time and nominal VLA parameters, is the minimum thermal noise expected in the map, assuming each data point to be weighted equally.

about as much as possible (beam solid angle halved), while no more than doubling the amplitude of the inner sidelobes. Maps using UVBOX = 4 (denoted 80DEC4 and 82MAY4) were made from the self-calibrated visibilities, and are used below (along with the UVBOX = 1 maps) to determine the structure of the G source and the B quasar. Parameters of the observations and resulting maps are summarized in Table 1.

Finally, in order to gain further confidence that the important low-level features of the maps are not artifacts of the CLEAN or ASCAL procedures, each data set was reprocessed several ways, using different CLEAN gains (0.1, 0.2) and cell sizes (0\".075, 0\".1). In no case did the features derived from the maps change in a significant way.

A self-calibrated map (80DEC1) of the entire double quasar field is shown in Figure 1. The principal features are the two bright quasar images A and B, the source G lying about 1\" north of B and closely coincident with the foreground galaxy G1, the jet extending 2\" northeast of A, and the related extended sources C, D, and E. In order to display a wide dynamic range without crowding the contours, logarithmic intervals are used, going by factors of 2 from 0.5 to 64 and then 95% of the 33 mJy per beam peak brightness (at A).

For completeness, the flux and position of the A quasar at these epochs are given in Table 2.

The small radio source G is already known to lie very close to the optical nucleus of the primary lens galaxy G1 and has been suggested as a candidate for the third quasar image (Greenfield, Burke, and Roberts 1980; Young *et al.* 1981). Thus given the new data in this paper, the important question to be answered are: (1) Is G the third quasar image B2? (2) If G is not B2, what is G, and what limits can one place on the flux and position of B2? (3) What is the relationship of G to the third VLBI component G′? In order to attack these questions, the flux, location, and angular structure of the G radio source were determined by model-fitting to the VLA maps, and the results compared to the optical position of the nucleus of the galaxy G1 to the VLBI structure of 0957+561 and to the predictions of models for the gravitational lensing in 0957+561.

IV. REGISTRATION OF THE OPTICAL, VLA, AND VLBI MAPS OF 0957+561

Figure 2 shows large-scale representations of the B-G regions of the two highest resolution maps of the double quasar 0957+561, with contour levels extending down to 0.25% of the peak. On these are plotted the positions of the third VLBI source G′ (Gorenstein *et al.* 1983) and of the optical nucleus of the primary lens galaxy G1 (Stockton 1980). Source B, used as the positional reference, has clear VLBI structure, so

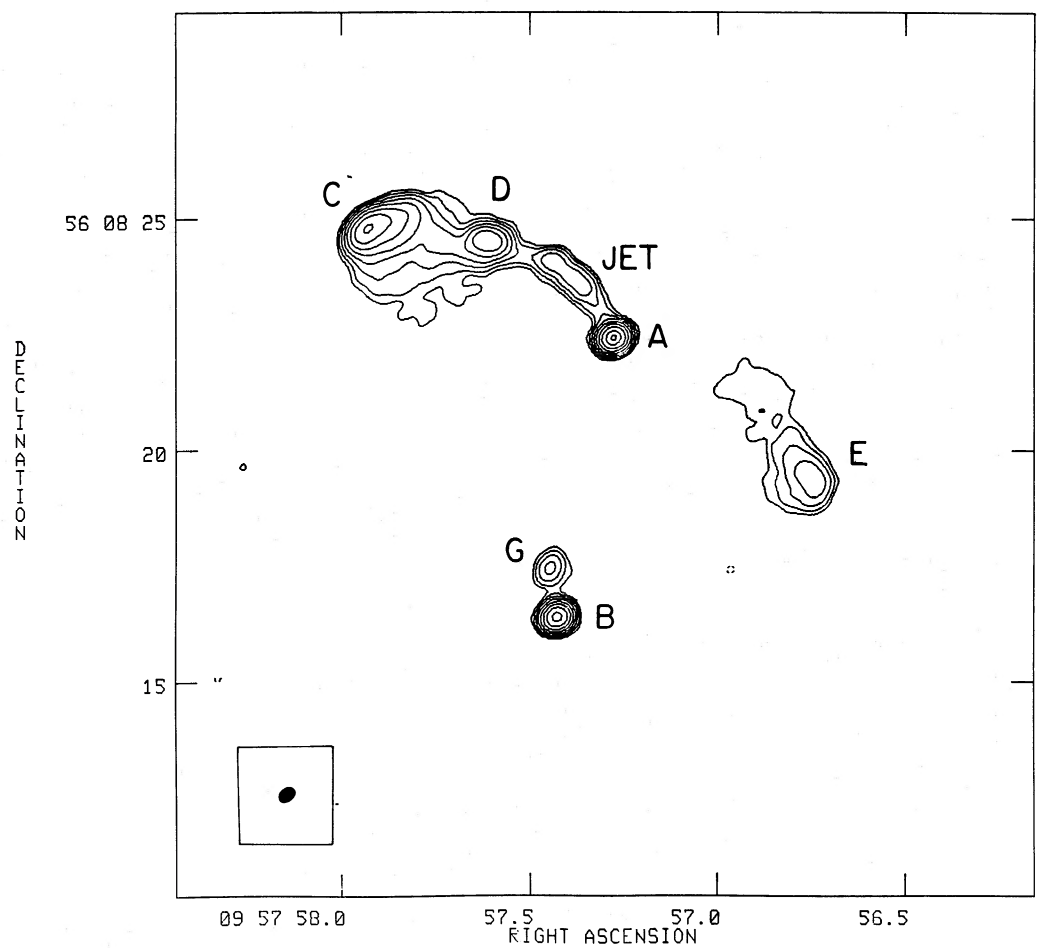

FIG. 1.—Self-calibrated 6 cm VLA map of the double quasar 0957+561, epoch 1980 December 16. The map has been restored with an ellipsoidal Gaussian clean beam with full-width at half-maximum of 0\".40 × 0\".35 at position angle 120°, corresponding to the true resolution of the observation, as shown in the box in the corner. Contour levels are −0.5, 0.5, 1, 2, 4, 8, 16, 32, 64, and 95% of the peak brightness (at A) of 33.3 mJy per beam area.

TABLE 2

A. Gaussian Fits to A and the B-G Regions of 0957+561

Component	Parameter	80DEC1	80DEC4	82MAY1	82MAY4
A	R.A.	-1.248 ± 0.001	-1.249 ± 0.001	-1.250 ± 0.001	-1.249 ± 0.001
	Decl.	6.044 ± 0.001	6.043 ± 0.001	6.043 ± 0.001	6.044 ± 0.001
	Flux	35.9 ± 0.4	36.0 ± 0.3	32.9 ± 0.3	32.9 ± 0.2
B	Flux	27.2 ± 0.1	27.1 ± 0.1	24.1 ± 0.1	24.1 ± 0.1
BN	R.A.	0.053 ± 0.008	0.092 ± 0.010	0.024 ± 0.008	0.036 ± 0.007
	Decl.	0.362 ± 0.013	0.355 ± 0.011	0.383 ± 0.014	0.311 ± 0.008
	Flux	0.31 ± 0.02	0.26 ± 0.02	0.40 ± 0.02	0.42 ± 0.03
			Model 1		
G	R.A.	0.148 ± 0.002	0.151 ± 0.002	0.151 ± 0.002	0.152 ± 0.002
	Decl.	1.050 ± 0.002	1.051 ± 0.002	1.049 ± 0.002	1.055 ± 0.003
	Flux	2.55 ± 0.11	2.40 ± 0.15	2.21 ± 0.15	2.00 ± 0.15
	Size	0.36×0.18 @ 164°	0.34×0.14 @ 163°	0.33×0.15 @ 168°	0.30×0.09 @ 168°
	rms (μJy)	36.4	39.1	45.4	47.4

B. Mean Values

	⟨R.A.⟩	⟨Decl.⟩	⟨Size⟩	⟨Flux⟩ 80DEC	⟨Flux⟩ 82MAY	⟨Flux⟩ All
A	-1.249 ± 0.001	6.044 ± 0.001	...	35.9 ± 0.2	32.9 ± 0.2	...
B	...	...	...	27.2 ± 0.1	24.1 ± 0.1	...
BN	$+0.05 \pm 0.02$	0.35 ± 0.02	...	0.28 ± 0.02	0.41 ± 0.02	0.34 ± 0.04
G	$+0.151 \pm 0.001$	1.051 ± 0.001	0.33×0.14 @ 166°	2.50 ± 0.09	2.14 ± 0.11	2.34 ± 0.12

Note.—Positions (in arc seconds) are given relative to the B quasar, whose position is found to be

$$\alpha = 09^{h}57^{m}57^{s}.42 \pm 0^{s}.02 , \quad \delta = 56°08'16''.4 \pm 0''.2 \ (1950.0) ,$$

and whose positional uncertainty is that of its phase calibrator 1031 + 567. Fluxes are in millijanskys.

the slight positional shifts due to the differing resolutions of the VLA and VLBI observations must be taken into account, as follows.

a) Position of the Third VLBI Source G′ in the VLA Map

The 13 cm VLBI of Gorenstein *et al.* (1983) has shown that there is a compact source (which they call G′), smaller than 2 mas and containing flux 0.6 ± 0.1 mJy, lying $0''.181 \pm 0''.001$ east and $1''.029 \pm 0''.001$ north of the compact core of B. The VLA position of B and the VLBI position of the core of B will differ somewhat because of the VLBI resolution of the source. At 18 cm wavelength the VLBI structure of B is core and jet, with fluxes of 24 and 17 mJy respectively, 56 mas separation, and core-jet position angle of 17° (Porcas *et al.* 1981). The 13 cm VLBI structure is quite similar, with core and jet fluxes of 19 and 22 mJy, separation of 50 mas, and position angle 15° (Gorenstein *et al.* 1983; Gorenstein and Rogers 1982). At both wavelengths the total VLBI flux on the shortest baselines was constrained with the 6–18 cm arc second spectrum of B (Noble and Walsh 1980; Greenfield, Roberts, and Burke 1985). This forced the models fitted to the VLBI data to place all the flux not in the unresolved core of B in the jet, so even though the jet is resolved by the VLBI observations, it is unlikely that much of its flux went unmodeled. However, the VLBI jet may be weaker relatively at 6 cm, since the correlated flux of B detected along much of a single 2 mas resolution *u-v* track by Porcas *et al.* was roughly constant and comparable to that measured for B at the VLA at same epoch (Porcas *et al.* 1981; Greenfield, Burke, and Roberts 1980). Allowing for a jet spectral index steeper than that of the core by between zero and one, the 13 cm VLBI core of B should lie 4–8 mas west and 15–27 mas south of the 6 cm VLA centroid of B, larger displacements occurring for smaller spectral index differences. The anticipated separation of G′ from B in our maps is thus $0''.175 \pm 0''.002$ east and $1''.008 \pm 0''.006$ north. Error boxes centered on this position with twice these uncertainties are plotted in Figures 2 and 3.

b) Position of the Lens Galaxy G1 in the VLA Map

Stockton's (1980) position for the optical nucleus of the primary lens galaxy G1 is $0''.19 \pm 0''.03$ east and $1''.00 \pm 0''.03$ north of the optical B quasar image. Since it is natural to associate the optical center of activity of the quasar with the VLBI core, the nucleus of G1 is positioned on the VLA map in the same way as was the third VLBI source G′, i.e., with respect to a point 6 mas west and 21 mas south of the VLA centroid of B. Thus in Figures 2 and 3 the optical nucleus of G1 is represented by a 2 σ error box centered $0''.18$ east and $0''.98$ north of B.

c) Anticipated VLA Flux of G′ If G′ Is the Third Quasar Image

If the 13 cm VLBI source G′ is a VLBI detection of the third image of the quasar, then the 6 cm VLA flux of G′ may be predicted from the G′/B intensity ratio of the VLBI images and the 6 cm VLA flux of B. In order to do so, one must know exactly what part of the third VLBI image (core, or jet, or core plus jet) the observed third VLBI source G′ represents.

It seems likely that if G′ is part of the third quasar image, then it is the core only: If G′ is the third image of the core alone, then the brightness ratio of the B2 to B1 images is equal to (flux of G′)/(flux of core of B) = 0.6/19 = 0.032. Since surface

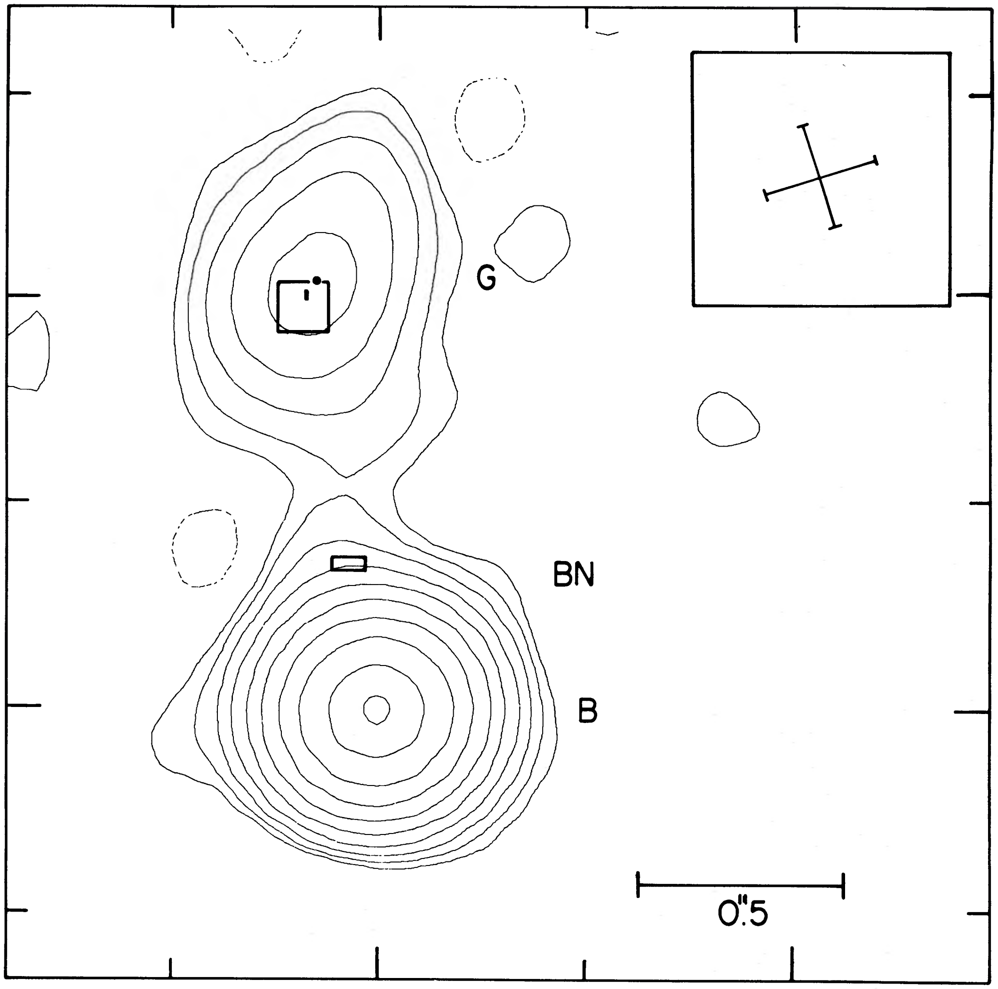

FIG. 2*a*

FIG. 2.—Self-calibrated super-uniform-weighted 6 cm VLA maps of the B-quasar region of the double quasar 0957+561. (*a*) Map 80DEC4, made from the same data as Fig. 1 but with more weight given to the longer interferometer spacings, was restored with clean beam 0."29 × 0."27 at position angle 118°, as shown in the box. Contour levels are −0.5, −0.25, 0.25, 0.5, 1, 2, 4, 8, 16, 32, 64, and 95% of the peak brightness (at B) of 25.7 mJy per beam area. (*b*) Map 82MAY4, made from an independent data base, has clean beam 0."27 × 0."25 at position angle 161°, as shown in the box. The contour levels are the same percentages of the peak brightness, which here is 22.2 mJy per beam area. The rectangles about 0."35 north of B are 2 σ error boxes for the small radio source BN which is responsible for the distortions of the lowest three contour levels in that region. The 2 σ error box for the optical nucleus of the galaxy G1 (Stockton 1980) is shown by the square which lies southeast of the centroid of the source G, which itself is marked by a solid dot. The small rectangle within the optical error box is the anticipated position of the third VLBI source G′ at the frequency and resolution of the VLA observations. The size of the rectangle represents twice the uncertainties in its position due to our imperfect knowledge of the relative strengths of the VLBI core and jet of B at 6 cm wavelength. Both the optical and VLBI positions have been shifted 6 mas west and 21 mas south to account for the different locations of the B quasar in the VLA, optical, and VLBI observations.

brightness is conserved in gravitational-image formation, intensities scale with the area of images, so that (as long as the image formation is not too astigmatic) linear sizes scale with the square root of intensities. Thus linear sizes at B2 will be smaller than those at B1 by $\sqrt{0.032} = 0.18$. Given this, the B2 image of the VLBI jet would contain 0.7 mJy in an area about 2 × 7 mas lying 9 mas south of G′. Such a third image of the VLBI jet might well have escaped detection, since the experiment of Gorenstein *et al.* had a fringe spacing of 3.5 mas and barely enough sensitivity to detect the 0.6 mJy point component G′.

On the other hand, if G′ is assumed to be the third image of the combined VLBI core and jet, the B2/B1 intensity ratio is G′/(B core + B jet) = 0.6/(19 + 22) = 0.015, and linear sizes at B2 would be smaller than those at B1 by a factor of 0.12. The observed source G′ would then have to consist of core of 0.3 mJy plus a jet about 2 × 5 mas also containing about 0.3 mJy, separated by about 6 mas. Since this leads to an inconsistency, it follows that if G′ is the third image B2, then it is the third image of the core only, and the B2/B1 intensity ratio as measured by VLBI is 0.032 ± 0.005. Thus *if G′ is the third quasar image*, its anticipated VLA flux at 6 cm is 0.86 mJy for 1980 December and 0.76 mJy for 1982 May. Note that B2/B1 = 0.032 ± 0.005 is in modest disagreement with Stockton's optical limit of 0.02 B1 on the intensity of any quasar images near the nucleus of the galaxy G1, but that this could be explained by as little as 0.5 mag of optical extinction.

V. MODEL FITS TO THE RADIO SOURCE G

Source G in Figures 1 and 2 is clearly more extended than either the A or B quasar (remember that the contours are logarithmic), and this is confirmed quantitatively in a series of

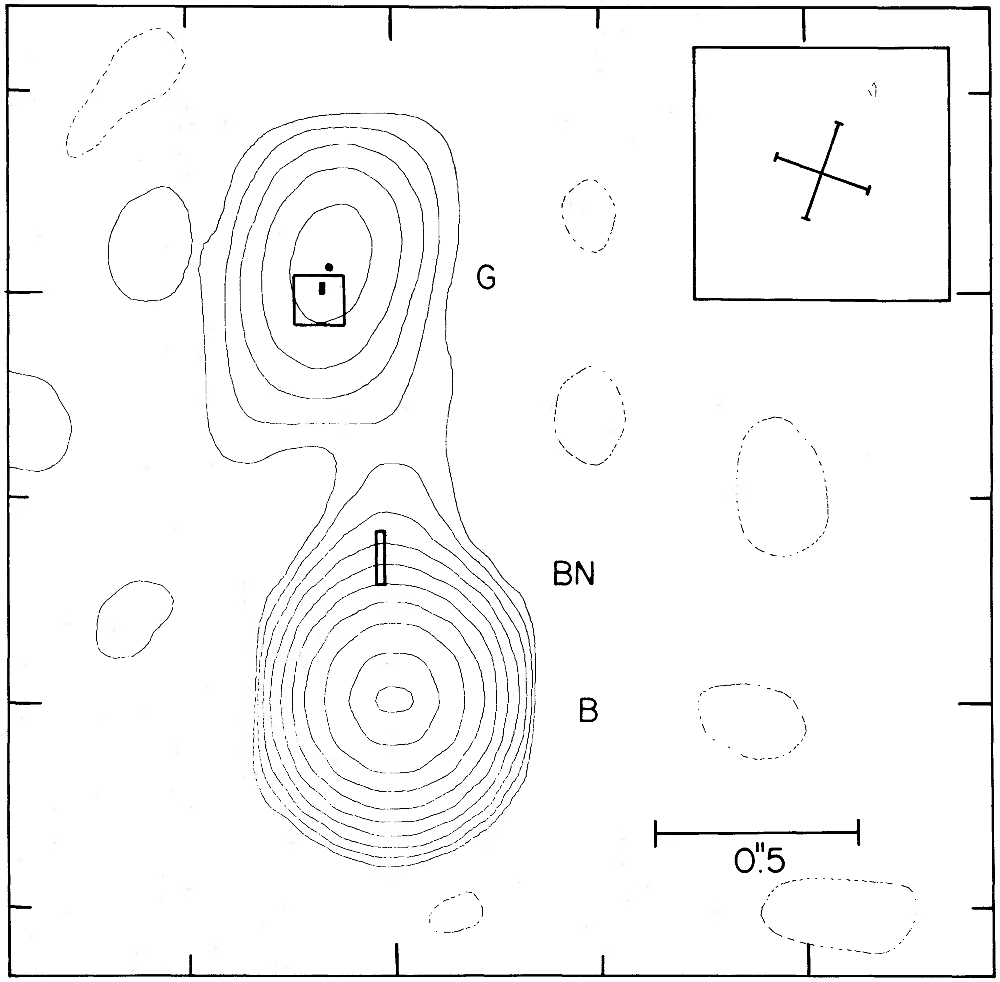

FIG. 2b

six models fitted to G. This was done using the standard AIPS Gaussian fitting routine IMFIT; the results are collected in Tables 2 and 3. The uncertainties quoted are those reported by the IMFIT routine and may be somewhat optimistic, especially regarding positions. However, in most cases averages over two or more maps are also given, and in those cases the internal dispersion of the fitted parameters has been considered in calculating the overall uncertainties. The positions of the model components, along with those of the optical nucleus of G1 and the third VLBI source G′, are shown in Figure 3. A detailed discussion of the models is given in the Appendix.

a) Summary of Six Models Fitted to Radio Source G

Model 1.—An examination of Figure 2 suggests that a single ellipsoidal Gaussian brightness distribution should work well. In the model, the position, flux, dimensions, and orientation were taken as free parameters. A satisfactory description of the (deconvolved) G source is a single Gaussian, 0."33 × 0."14 (FWHM) with major axis position angle 166°.

Model 2.—Models with an elliptical Gaussian plus an unconstrained point source provide the best fits to the data but are inconsistent between the two epochs. In no case is the point source located in the expected position of the third quasar image B2 (south of the optical nucleus of G1), nor does it lie on the third VLBI source G′.

Model 3.—One possible origin of the extended nature of G is that it is composed of two distinct sources, one due to emission from the lens galaxy G1 plus a second due to the third quasar image B2. This model, accordingly, contained two unconstrained point sources. The resulting fits to the data are all inferior to those of model 1, and the sources lie neither on the optical nucleus of G1 nor on the third VLBI component G′.

Model 4.—Whether the third VLBI source G′ is the third quasar image B2 or is intrinsic to G1, it must be present in the VLA map at some level. The two-point model 3 (above) was therefore constrained to have one of the point sources located at G′, both sources having arbitrary flux. The residuals for this model are considerably worse than for models 1, 2, or 3, and the free point model are considerably worse than for models 1, 2, or 3, and the free point source consistently lies significantly north of the optical nucleus of G1.

Model 5.—This is a generalization of model 4, consisting of a point source of arbitrary flux fixed at G′ plus an unconstrained elliptical Gaussian. This model yields inconsistent results, the fitted fluxes for the point source being negative in each of the 1982 May maps, while the models derived from the two 1980 December maps do not agree with each other.

Model 6.—The final model was a test of the consistency of the hypothesis that the third VLBI source G′ is the third quasar image B2. Model 5 was further constrained by fixing

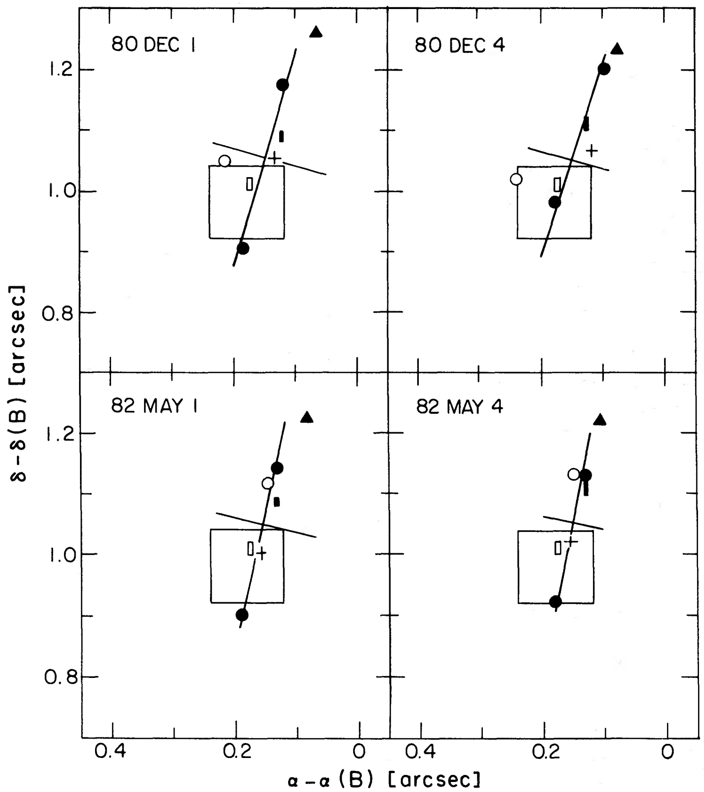

FIG. 3.—Schematic representations of the models which are fitted to the G radio source. All positions are relative to the VLA centroid of the B quasar. The 2 σ error boxes for the optical nucleus of the lens galaxy G1 and the anticipated VLA position of the third VLBI source G′ are the large open square and small rectangle within it, respectively, as in Fig. 2. The large crosses show the full-widths and orientations of best-fit single elliptical Gaussians (Model 1 of Table 2). The small crosses and open circles locate the best-fit Gaussian and point components respectively in a model in which none of the parameters are constrained (Model 2 of Table 3). The filled circles mark the best-fit positions of two unconstrained point sources (Model 3). The triangles are the positions of a second point source required when a first point source of unconstrained flux is forced to lie at the anticipated position of the third VLBI source G′ (Model 4). Finally, the solid rectangles indicate the range of location of the centroids of the elliptical gaussian components when a point source with flux within 10% of that predicted (by the VLBI ratio G′/B) for the third quasar image is put at the anticipated VLA position of G′ (Model 6).

the flux of the point component to be within 10% of the expected 6 cm VLA flux of G′ (see § IV*c*). While the model are acceptable, in all cases there is a clear preference for a point component smaller than that anticipated. This suggests that, if G′ is the third quasar image, the structure of the remainder of G (intrinsic to the galaxy G1) is more complex than a simple elliptical Gaussian.

b) Discussion of the Model Fits to G

The small radio source G may be fitted by a variety of models consisting of one or more point or elliptical or both Gaussian components. A satisfactory fit can be obtained with a single Gaussian 0″33 × 0″14 FWHM with major axis position angle of 166°. Comparison of the resolution-corrected positions of the optical centroid of the galaxy G1, the third VLBI source G′, and the centroid of the radio source G yields:

$$\alpha(\mathrm{G1}) - \alpha(\mathrm{G}) = +0''.03 \pm 0''.03 \ ,$$
$$\delta(\mathrm{G1}) - \delta(\mathrm{G}) = -0''.07 \pm 0''.03 \ ,$$

$$\alpha(\mathrm{G}') - \alpha(\mathrm{G}) = +0''.024 \pm 0''.002 \ ,$$
$$\delta(\mathrm{G}') - \delta(\mathrm{G}) = -0''.043 \pm 0''.006 \ ,$$

$$\alpha(\mathrm{G1}) - \alpha(\mathrm{G}') = +0''.01 \pm 0''.03 \ ,$$
$$\delta(\mathrm{G1}) - \delta(\mathrm{G}') = -0''.03 \pm 0''.03 \ .$$

Thus, unless the optical position of G1 is badly in error, some of the flux from the radio source G lies north of the nucleus of the lens galaxy G1. Since models with three gravitational images requires both images in this region (B1 and B2) to lie south of the nucleus of the galaxy, *at least some of the flux in radio source G is not due to the third gravitational lens image.* This may be concluded independent of any uncertainties about the location of the optical nucleus, simply from the extended nature of G; since the third quasar image B2 is fainter than the A or B1 images, it must be smaller, and thus must be unresolved by the VLA.

The third VLBI component G′ lies slightly but significantly south and east of the centroid of radio source G. The positions of the optical galaxy nucleus G1 and the third VLBI source G′ are coincident within the uncertainties.

Attempts to locate B2 by including arbitrary point sources do not lead to an unambiguous result but may be used to place limits on the brightness ratio of the quasar images, B2/B1 (see § VI).

Models consisting of a point source constrained to lie at the position of the third VLBI source G′ plus a simple model for the remainder of the source G galaxy G1 are not very successful. Models with two point sources, one lying at G′, fail to account for all the flux in G. Addition of a point source at G′ to ellipsoidal Gaussian models of G leads both to larger residuals and to inconsistent (and sometimes nonphysical) fluxes for the

TABLE 3

MULTIPLE-COMPONENT MODELS FOR THE G RADIO SOURCE

Component	Parameter	80DEC1	80DEC4	82MAY1	82MAY4
		Model 2			
Gauss	R.A.	0.136 ± 0.005	0.121 ± 0.004	0.157 ± 0.008	0.155 ± 0.009
	Decl.	1.051 ± 0.004	1.067 ± 0.005	1.001 ± 0.011	1.023 ± 0.011
	Flux	2.26 ± 0.37	1.91 ± 0.24	1.59 ± 0.40	1.64 ± 0.32
	Size	0.39 × 0.18 @ 165°	0.39 × 0.09 @ 170°	0.40 × 0.20 @ 166°	0.33 × 0.11 @ 166°
Point	R.A.	0.215 ± 0.038	0.243 ± 0.011	0.145 ± 0.014	0.148 ± 0.028
	Decl.	1.048 ± 0.017	1.019 ± 0.008	1.115 ± 0.016	1.131 ± 0.020
	Flux	0.31 ± 0.11	0.51 ± 0.06	0.67 ± 0.09	0.44 ± 0.09
Total flux		2.57 ± 0.38	2.42 ± 0.25	2.26 ± 0.41	2.08 ± 0.33
rms (μJy)		36.1	36.9	44.2	46.5
		Model 3			
GN	R.A.	0.115 ± 0.005	0.098 ± 0.005	0.131 ± 0.003	0.134 ± 0.002
	Decl.	1.172 ± 0.007	1.196 ± 0.007	1.138 ± 0.006	1.135 ± 0.005
	Flux	1.19 ± 0.04	0.85 ± 0.03	1.25 ± 0.05	1.16 ± 0.04
GS	R.A.	0.182 ± 0.005	0.179 ± 0.003	0.185 ± 0.005	0.182 ± 0.003
	Decl.	0.929 ± 0.008	0.977 ± 0.005	0.899 ± 0.010	0.925 ± 0.006
	Flux	1.18 ± 0.04	1.33 ± 0.03	0.82 ± 0.05	0.79 ± 0.04
Total flux		2.37 ± 0.06	2.17 ± 0.04	2.07 ± 0.07	1.95 ± 0.06
rms (μJy)		43.0	45.2	48.4	51.4
		Model 4			
GN	R.A.	0.067 ± 0.010	0.077 ± 0.005	0.086 ± 0.006	0.108 ± 0.005
	Decl.	1.257 ± 0.011	1.234 ± 0.006	1.218 ± 0.010	1.191 ± 0.006
	Flux	0.63 ± 0.02	0.65 ± 0.02	0.57 ± 0.02	0.68 ± 0.02
G′	R.A.	0.175	0.175	0.175	0.175
	Decl.	1.008	1.008	1.008	1.008
	Flux	1.68 ± 0.02	1.50 ± 0.02	1.42 ± 0.03	1.21 ± 0.03
Total flux		2.31 ± 0.03	2.15 ± 0.03	1.99 ± 0.04	1.89 ± 0.04
rms (μJy)		53.1	48.1	55.9	58.0
		Model 5			
Gauss	R.A.	0.147 ± 0.002	0.143 ± 0.003	0.158 ± 0.003	0.158 ± 0.002
	Decl.	1.052 ± 0.003	1.065 ± 0.005	1.039 ± 0.005	1.043 ± 0.005
	Flux	2.49 ± 0.26	2.04 ± 0.25	2.76 ± 0.49	2.58 ± 0.41
	Size	0.36 × 0.18 @ 164°	0.38 × 0.15 @ 164°	0.29 × 0.13 @ 168°	0.27 × 0.08 @ 168°
G′	R.A.	0.175	0.175	0.175	0.175
	Decl.	1.008	1.008	1.008	1.008
	Flux	0.06 ± 0.11	0.37 ± 0.07	−0.56 ± 0.28	−0.53 ± 0.22
Total flux		2.55 ± 0.28	2.41 ± 0.26	2.20 ± 0.56	2.05 ± 0.47
rms (μJy)		37.4	38.7	45.4	49.8
		Model 6			
Gauss	R.A.	0.125 ± 0.004	0.125 ± 0.005	0.132 ± 0.004	0.131 ± 0.003
	Decl.	1.088 ± 0.006	1.100 ± 0.009	1.086 ± 0.006	1.107 ± 0.011
	Flux	(1.62–1.80) ± 0.15	(1.47–1.65) ± 0.19	(1.39–1.54) ± 0.18	(1.19–1.37) ± 0.21
	Size	0.45 × 0.22 @ 167°	0.44 × 0.16 @ 166°	0.42 × 0.19 @ 170°	0.35 × 0.11 @ 170°
G′	R.A.	0.175	0.175	0.175	0.175
	Decl.	1.008	1.008	1.008	1.008
	Flux	0.86 ± 10%	0.86 ± 10%	0.76 ± 10%	0.76 ± 10%
Total flux		2.57 ± 0.15	2.42 ± 0.19	2.23 ± 0.18	2.04 ± 0.21
rms (μJy)		39.8–41.4	40.4–42.6	48.0–49.2	55.2–57.2

NOTE.—Model 2 consists of an unconstrained elliptical Gaussian plus an unconstrained point source. Model 3 has two unconstrained point sources. Model 4 has one unconstrained point source and one point source constrained to be at the anticipated VLA position of the third VLBI source G′. The position of this source thus has "no" uncertainty. In Model 5 a point source fixed at G′ is fitted simultaneously with an unconstrained elliptical Gaussian. Model 6 fixes the flux at G′ to be that anticipated if G′ is the third quasar image; the uncertainties quoted are for variations of ± 10% in the VLA flux of G′.

VLA analog of G′. And finally, models which include a third quasar image whose position and flux are determined by the hypothesis that the third VLBI source G′ is the third quasar image lead to rather poor fits to the VLA data. It should be emphasized, however, that there is more flux at the appropriate position in G than is required by this hypothesis, so it is consistent with the VLA data.

VI. GRAVITATIONAL LENS PREDICTIONS FOR THE THIRD IMAGE B2

In the models of Young *et al.* and of Greenfield, Roberts, and Burke, the position and flux of the third quasar image B2 depends almost entirely on the structural length a of the primary lens galaxy G1 (a = galaxy core radius/3). Figure 4 shows the predicted brightness ratio of the two southern quasar images (B2/B1) versus their declination separation, as parameterized by a (Greenfield, Roberts, and Burke 1985). One set of models assumes that the separation of the B1 quasar image and the nucleus of the primary lens galaxy G1 is 1″.0, as measured by Stockton. The second set is appropriate to the slightly greater declination difference of 1″.1. These model predictions are compared to various limits on B2/B1, derived by assuming that the third image B2 is: (1) the VLBI source G′ (the core of B2), (2) the point component of a point-plus-Gaussian model for G (POINT in Model 2), (3) either a pair of points fitted to G (GN and GS in Model 3), or (4) a point fixed at G′ as part of a model of G (POINT in Models 4 and 5). Also shown is a smooth curve derived from the observed (not deconvolved) cross section along the major axis of the G source, taken from the 82MAY4 map, in order to exhibit explicitly the actual flux levels involved in the fitting.

Comparison of the theoretical models with the data suggests that none of the identifications (1) through (4) is viable, even in the case $\delta(G1) - \delta(B) = 1''.1$: (1) This agrees with the suggestion of Gorenstein *et al.* (1983) that the VLBI source G′ may be too close to the nucleus of G1 for G′ to be the third image. (2) The free point sources in Model 2 are not only too bright, they lie north of the nucleus of the lens galaxy G1. (3) and (4) The point

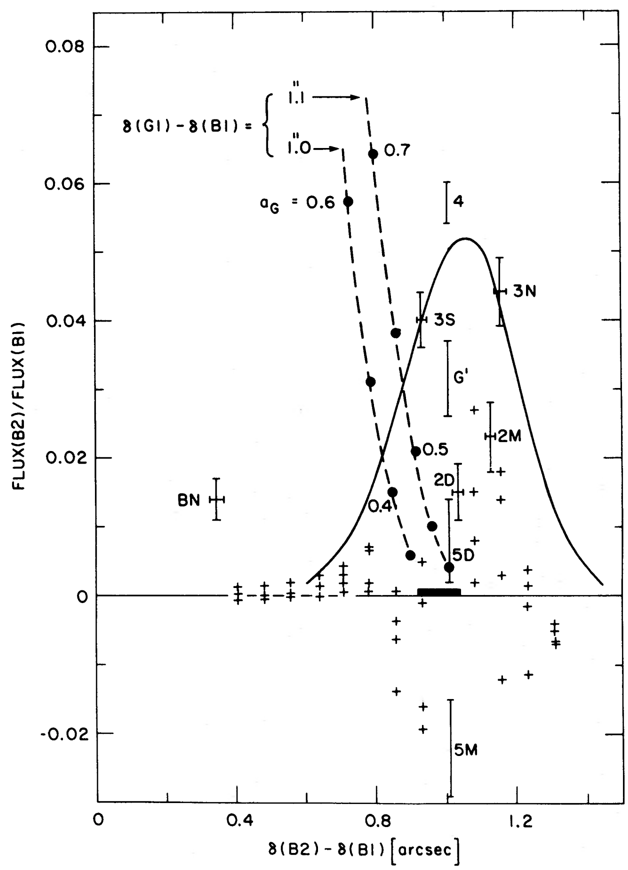

FIG. 4.—Brightness ratio versus declination separation for gravitational-lens models and for VLA and VLBI observations of the southern quasar region of the double quasar 0957+561. The theoretical points (see Greenfield, Roberts, and Burke 1985) are labeled by the declination separation assumed between the bright B1 quasar image and the nucleus of the lens galaxy G1, and by the scale length assumed for the primary lens galaxy G1 (a_G in kpc, in steps of 0.1). The model points are joined by broken lines to guide the eye. The location (with 2 σ uncertainty) of the optical nucleus of the lens galaxy G1 is indicated by the heavy bar along the abscissa. Several candidates for the third quasar image B2 are plotted on the same scale. The observed 13 cm VLBI ratio (third source G′/B quasar core) is labeled G′. The points labeled 2 through 5 refer to empirical models fitted to the VLA observations of the radio source G (see Table 3 and Fig. 3, and Appendix). Where the 1980 December and 1982 May maps yield significantly different results they are plotted separately, and denoted "D" and "M" respectively. For Model 3, each of the pair of points is shown (GN and GS are labeled "3N" and "3S"). In Models 4 and 5 the point source fixed at the anticipated VLA position of G′ is taken as the candidate B2, while for Model 2 the unconstrained point component is used. The crosses (+) represent the results of fitting an unconstrained elliptical Gaussian plus a point source, when the latter is constrained to a series of positions between 0″.3 north and 0″.6 south of the nucleus of G1, i.e., along the locus of expected positions for a third quasar image. The smooth curve is the (nondeconvolved) cross section through the major axis of G in the radio map 82MAY4 and illustrates the actual flux levels in the data.

sources in Models 3 and 4 are too close to the nucleus of G1 to be as bright as they are. In general, *the bulk of the flux in radio source G lies too close to the nucleus of the lens galaxy G1 for any substantial part of G to be the third quasar image predicted by the models.* An optical separatiion of B and G1 of at least 1″.2 is required in order that the "southern half" of G be the third quasar image predicted by the theoretical models, but this appears to be in strong conflict with Stockton's measurement of the position of G1.

a) Limits on the Flux of a Third Quasar Image B2 Located South of the Nucleus of G1

In the absence of successful identification of the third quasar image B2 in radio source G, it is possible to derive limits on B2 as a function of its separation from the nucleus of G1. Two sets of models were used to find such limits. The first added a point source at predetermined positions to the Gaussian component of Model 1 and fitted the flux of the point component. The point source was moved along a north-south line passing through the VLA anticipated position of G′ in steps of one map cell = 0″.075, from four cells (0″.3) north of G′ to eight cells (0″.6) south. This line passes very close to Stockton's position for the optical nucleus of G1, and is the locus of predicted third image positions. The resulting limits on B2 were always within the rms residuals to the fits of Model 1, and correspond to limits on B2/B1 consistently less than 0.002 for all B2-B1 separations sampled.

The second series of models used point sources located on the same line, but permitted an arbitrary Gaussian component. The resulting limits on B2/B1 are shown as the crosses in Figure 4; the four values of B2/B1 plotted at each position correspond to the four maps fitted. The brightest point source permitted south of the galaxy G1 is 0″.2 from the nucleus and has intensity ratio B2/B1 ≈ 0.007. This is consistent with the theoretical models only if $\delta(\mathrm{G1}) - \delta(\mathrm{B}) \approx 0''.8$ and $a_G < 0.4$ kpc, both of which are in strong disagreement with Stockton's measurements.

b) Intrinsic Properties of Radio Source G Compared to Those of M87

The 6 cm radio properties of G are not dissimilar to those which would be observed for the nearby giant elliptical galaxy M87 were it at the distance of G1. The central radio component of M87, having an apparent size about 40″ × 12″ and flux density of 55 Jy (Turland 1975), would exhibit angular size about 0″.7 × 0″.2 and flux density about 6 mJy. The extended halo of M87 would be too faint to be detected. The nucleus of M87 contains a VLBI core (1 Jy in 0.6 mas) and halo (1.2 Jy in 6 mas; Pauliny-Toth *et al.* 1981), plus 1.9 Jy additional flux which is probably in a jet 50 ms long (Turland 1975; Owen, Hardee, and Bignell 1980; Reid *et al.* 1982). At $z = 0.36$ this would all appear within a source less than 1 mas across containing about 0.4 mJy. The centroid of M87 and its VLBI core would be offset by 0″.1 due to its arc second asymmetry.

c) Conclusion about Radio Source G

The position and structure of G are inconsistent with its being *wholly* the third quasar image B2, and the bulk of the flux is probably due to a nuclear radio source in the primary lens galaxy G1. The assumption that G′ is the third quasar image B2 forces there to be a point source of known flux and position in the VLA map of G; although this is consistent with the data, the remainder of the radio source (intrinsic to the galaxy G1) would not have a simple structure. The third VLBI component G′ could also be the radio core of the lens galaxy G1. If the theoretical models of Greenfield, Roberts, and Burke describe correctly the possible positions and intensities of the third quasar image B2, it is confused with the (much brighter) intrinsic source in G1; B2 then probably lies within 0″.2 of the nucleus of the lens galaxy, and is less than 1% as bright as the B quasar image.

d) A Possible Alternative Interpretation

A gravitational lens with a nonsingular mass distribution need not produce three images—any old number is in principle possible. In particular, if the bending curve (angular deflection of light versus impact parameter) of the lens has both positive curvature and a sufficiently small slope for small positive impact parameters, five images can be formed. Thus not one but three images may be missing from 0957+561. This is not possible for a single, spherical King-model lens; in the notation of Young *et al.* (1980, 1981), it is easy to show that the bending curve has negative curvature near the origin for small β,

$$\frac{d^2\alpha^*}{d\beta^2} = -0.68\beta ,$$

where α^* and β are the scaled bending angle and dimensionless impact parameters respectively. However, since the additional bending contribution of the cluster is necessary in order to produce the apparently well-separated and very unequal B1 and B2 images in 0957+561, the question of whether or not five images are possible cannot be answered without the numerical calculations required of a more complete model. In fact, Young *et al.* (1980) showed explicitly that a quintuple image can occur if the quasar image which would be produced by the cluster alone lies sufficiently close to the primary lens galaxy G1. Thus it is useful to examine the second condition for five images, namely that of sufficiently small slope of the bending curve near the origin. This may be shown to enforce a condition on the scale length a and velocity dispersion σ_v^2 of the lens galaxy, and on the distances D_d, D_s, and D_{ds} involved, of the form

$$a > \left(\frac{6D_{ds}D_d}{D_s}\right)\left(\frac{\sigma_v}{c}\right)^2 .$$

It is interesting that this condition is met in the models of Greenfield, Roberts, and Burke, where $a = 0.35$–0.44 kpc and the right-hand side = 0.31 kpc.

The advantages of postulating five images in 0957+561 are several: The missing B images would be triple; it is likely that their sum would be resolved by the VLA. One or two of the missing images would lie north of the nucleus of the lens galaxy. The position angle of the triple of missing images would probably be similar to that of the line joining the A and B quasars (168°), which is remarkably close to that of the major axis of the G radio source (166°).

If G consists mostly of quasar images, its 6–18 cm radio spectrum should be similar to those of the A and B images. Greenfield, Roberts, and Burke (1985) have determined that in 1980 December the 18 cm fluxes of A, B, and G were 61.8 ± 1.7, 45.3 ± 1.0, and 4.2 ± 0.6 mJy respectively, where the errors are purely those derived by IMFIT from the noise in the maps. They do not include any allowances for an overall flux-scale error, which is irrelevant in comparison of the spectral indices of different sources in the same field. Using the

$\lambda = 6$ cm fluxes of Table 2, the 6–18 cm spectral indices of A, B, and G are -0.50 ± 0.03, -0.47 ± 0.02, and -0.47 ± 0.13 respectively. Thus the radio spectral information is compatible with the hypothesis that much of G consists of quasar images.

If the double quasar 0957+561 is really quintuple, then the radio flux ratio (total flux of G)/B $= 0.091 \pm 0.003$ for 1980 December and 0.089 ± 0.003 for 1982 May, with a grand average of 0.090 ± 0.003, predicts the total optical intensity of the three extra quasar images. Since Stockton has placed a limit of 2% of B on the B-band optical flux of any additional quasar image(s) at the position of the galaxy G1, the quintuple-image hypothesis is viable only if the corresponding optical images suffer 1.6 mag or more of extinction in passing through the lens galaxy. This hypothesis also predicts that the third VLBI component G′ is simply the brightest of a trio of nearly equal images.

Finally, if there is a massive black hole or other highly condensed object at the nucleus of the galaxy G1, there will be an even number (greater than or equal to four) of images in 0957+561. The case of four images does not have quasar images north of the nucleus of G1 and is therefore not promising. The six-image case has a "quadruple G," two images lying on either side of the nucleus of G1.

VII. STRUCTURE OF THE B QUASAR IMAGE

Examination of the two highest-resolution maps of the B-G region (80DEC4 and 82MAY4, Figs. 2*a* and 2*b*) reveals a slight distortion of the B-quasar contours at the three lowest levels (0.25–1% of B). The fitting of the B quasar with a single elliptical Gaussian always leaves a small residual source ("BN") which lies 0″.3–0″.4 north of B. Simultaneous fitting of B, G, and BN results in the fluxes and positions which are given in Table 2. An average over the results from the four maps locates the (point) source BN 0″.35 ± 0″.02 north and 0″.05 ± 0″.02 east of the bright B quasar image and yields a flux of 0.33 ± 0.04 mJy. When B, G, and BN are fitted simultaneously, the rms of the residual maps are comparable to the rms noise of the original maps (cf. Tables 1 and 2); this is not the case without inclusion of a source BN. The fact that this source is seen in two independent data sets processed in several ways makes it clear that it is not an artifact of the mapmaking process. (In fact, BN is visible in the first un–self-calibrated maps made from each data base, although at lower signal-to-noise ratio.) The error boxes for BN derived from the 1980 December and 1982 May maps are superposed on the 80DEC4 and 82MAY4 maps in Figures 2*a* and 2*b*.

a) Is BN the Third Quasar Image?

The hypothesis that BN is the third quasar image may be tested by comparing its flux and separation from the B1 image with that in the models of Greenfield, Roberts, and Burke (1985). This is done in Figure 4, and it is clear that *the source BN is much too weak to be the third image B2*. This conclusion is largely independent of the details of the gravitational lens models; as shown by Young *et al.* (1980), if B1 and B2 are very close together they will be comparable in size and thus in brightness. It seems likely that this would be the case even in a quintuple-image situation, but it ought to be checked—there might be quintuple models with two unequal images near B and two faint images near the nucleus of G1! Gorenstein and Rogers (1982) report that there is no λ-13 cm VLBI component in the vicinity of BN, to a threshold of 0.4 mJy. Interpretation of BN as a quasar image requires a λ-13 cm VLBI core at its location with a flux of 0.3 mJy, consistent with this upper limit.

b) Is BN an Additional Image of the Arc Second Jet Near A?

The models of Young *et al.* and of Greenfield, Roberts, and Burke predicted that a short spur of the VLA A-jet will have two additional images which will lie between the B1 and B2 quasar images. That section of the A-jet which is multiply imaged in Greenfield, Roberts, and Burke's model 3 is shown in Figure 5*a*; the corresponding images are superposed on the 82MAY 4 map in Figure 5*b*. The solid part is the second image and the open part the third image; their *predicted* λ-6 cm flux densities are 0.40 and 0.04 mJy respectively. The rectangular box shows the average position of BN as determined from all four maps. The model puts the third quasar image at the end of the third A-jet image; its flux density was fixed at 2% of B in order to satisfy Stockton's optical limit on B2/B1. Comparison of the observed position and flux of BN with that predicted for the additional A-jet images strongly suggests that at least one of these images has been found. Given the angular sizes and flux densities involved, it is not surprising that we cannot resolve BN into a jet with the current observations.

VIII. CONCLUSIONS

Very Large Array observations of the gravitationally lensed double quasar 0957+561, with resolution of 0″.3 and dynamic range of several hundred, have revealed new details of this complex source. Radio source G is resolved, and its centroid is found to lie slightly north of Stockton's position for the nucleus of the lens galaxy G1. Thus G cannot be wholly the required third quasar image, and most of its flux is probably intrinsic to the galaxy. Although the VLA flux and position of G are consistent with the hypothesis that the third VLBI source G′ is the third quasar image B2, models fitted to the structure of G do not unambiguously yield the anticipated point component. G′ may instead lie in the nucleus of the lens galaxy G1. The inferred VLA and VLBI radio properties of G1/G are quite similar to those of M87/Virgo A. The hypothesis that 0957+561 is actually a quintuple image, and that radio source G represents three additional quasar images, was considered, and found to be possible if there are as few as 1.6 mag of optical extinction in the nucleus of G1. The weak, new radio source BN discovered 0″.35 north of B is too faint to be the third quasar image but is probably the (predicted) additional image of the arc second jet whose first image lies northeast of A. There is no unambiguous evidence for the third quasar image in the VLA maps.

Deconvolution of the radio source G into the third quasar image and the intrinsic source in the galaxy (or into separate missing quasar images) might be possible with a VLA synthesis at 2 cm, using the newly installed FET receivers. Even if G is not fully resolved, a spectral index map might be telling—a strong gradient would rule out a quintuple-image interpretation and help separate the third image from the intrinsic source in the lens galaxy. Observations with the Space Telescope would appear to be necessary to improve the relative positions of the quasar image B and the nucleus of the lens galaxy G1 (and hence of the radio sources G and G′ with respect to G1), as well as to search for the additional quasar image(s). Finally, further gravitational-lens models should be explored in order to see if it is indeed possible to have five images in the "double quasar" 0957+561.

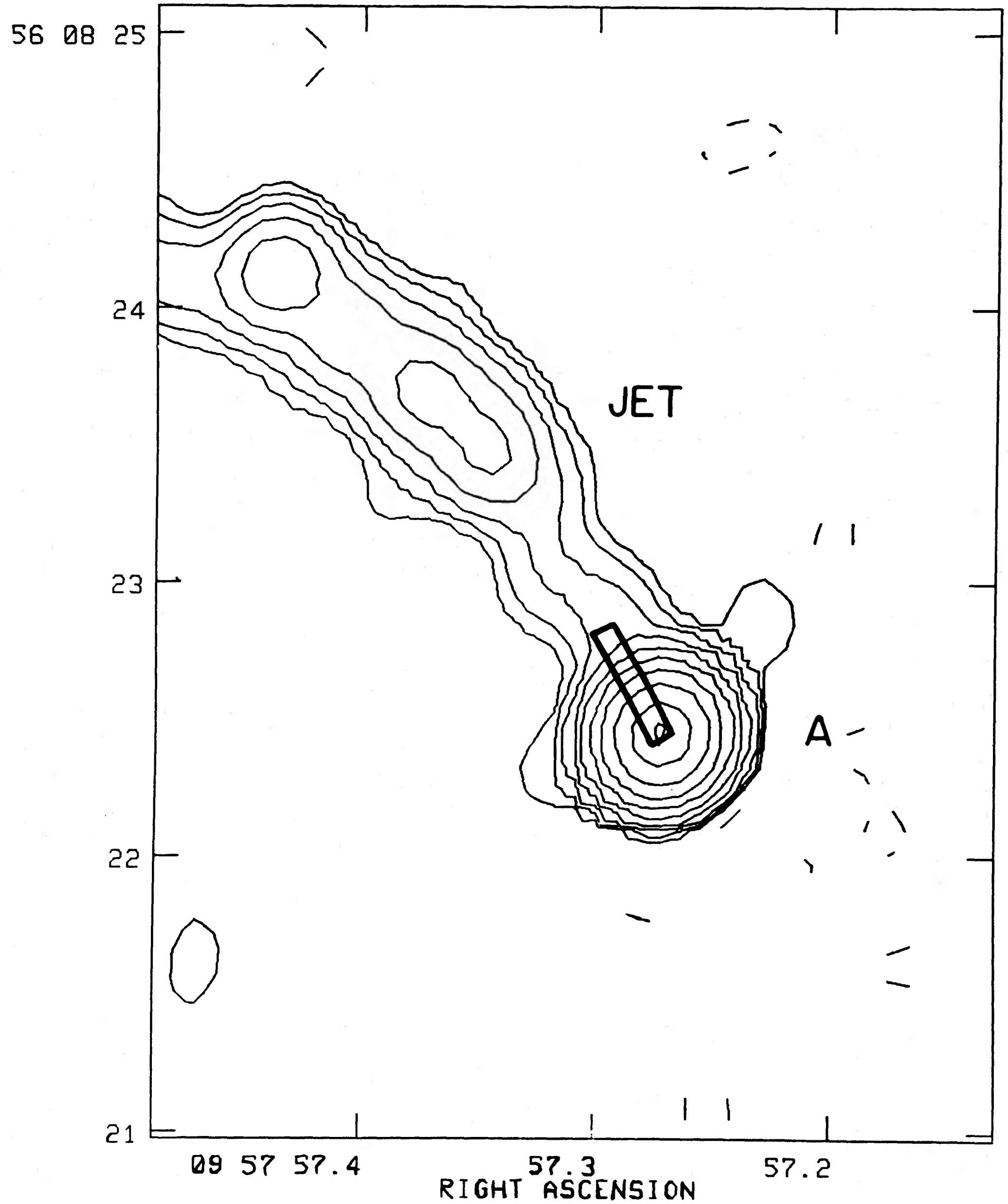

FIG. 5a

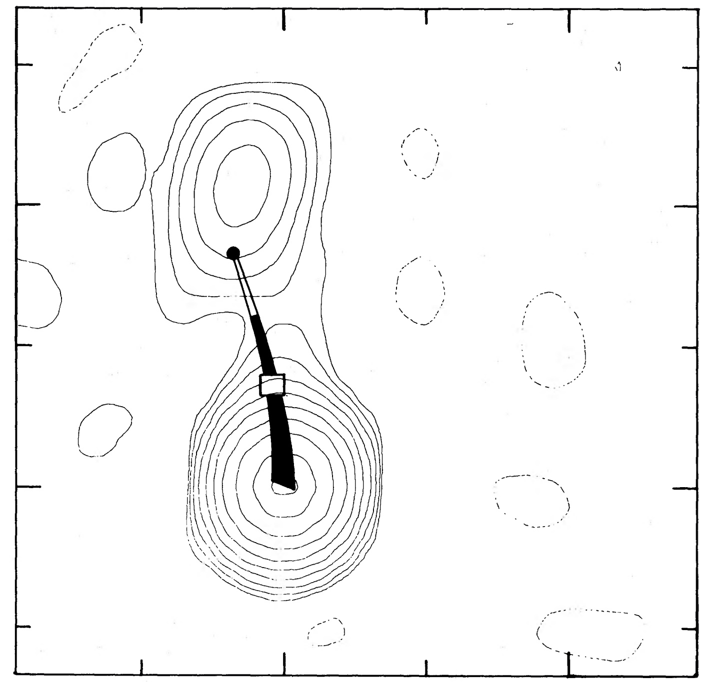

FIG. 5b

FIG. 5.—Images of the arc second radio jet. (*a*) VLA map 82MAY4 of the A-quasar and the jet, with contour levels −0.5, −0.25, 0.25, 0.5, 1, 2, 4, 8, 16, 32, 64, and 95% of the peak brightness (at A) of 29.8 mJy per beam. On this is outlined the section which is multiply imaged according to the model of Greenfield (1981). (*b*) VLA map 82MAY4 of the B-G region (same as Fig. 2*b*). Superposed is the predicted configuration of the second (*open*) and third (*solid*) images of the A-jet. The third quasar image is expected to lie at the end of the third jet image, as indicated by the dot. The open square is a 2 σ error box about the average position (from 1980 December and 1982 May data) of the small source BN. The two figures are to the same scale.

The research reported here was supported in part by a grant from the National Science Foundation. J. N. H. thanks Zonta International for an Amelia Earhart Fellowship. We are pleased to thank T. Cornwell and F. Schwab for their assistance with the self-calibration programs; M. Gorenstein, I. I. Shapiro, and A. E. E. Rogers for discussions concerning their VLBI observations; J. Dreher for useful suggestions on VLA data processing; J. Moran for generous loan of disk space; J. F. C. Wardle and A. E. E. Rogers for careful readings of the manuscript and helpful discussions; and D. Eckert for her skillful typing of the several versions of this paper.

APPENDIX

Here we describe in some detail the six models fitted to the radio source G.

a) Models Consisting of a Single Elliptical Gaussian (Model 1)

A point source does not provide a good representation of the G radio source; the simplest model which adequately fits G is a single unconstrained elliptical Gaussian (Model 1). An average of the results for the four maps yields (deconvolved) full-widths-at-half-maxima of $0''.33 \times 0''.14$ at position angle 166°. The residuals to these fits (see Table 2) are consistent with the measured noise in the maps. Models with an unconstrained elliptical Gaussian plus an unconstrained point source result in slightly smaller residuals, but the location of the point component is not consistent from map to map (see below, where this is denoted Model 2). In all cases the majority of the flux lies in the elliptical component, *and as long as one is simply seeking an adequate fit to the data*, there is no compelling need for this additional component. However, in order to derive limits on the intensity and location of a third quasar image, models consisting of various point and elliptical Gaussian components are fitted to radio source G in the sections below.

b) Point Plus Elliptical Gaussian (Model 2)

Models with an unconstrained point source plus an unconstrained elliptical Gaussian fitted to the remainder of G are denoted Model 2. These provide the best fits to the data of any of the models, but are inconsistent between the two epochs. In the 80DEC maps the point component lies east of the Gaussian one, while in the 82MAY maps it lies north. In no case does the point component fall naturally on the anticipated VLA position of the third VLBI source G′. However, the point components may be used to put limits on a third quasar image; $B2/B1 < 0.015 \pm 0.004$ for 1980 December and $B2/B1 < 0.023 \pm 0.005$ for 1982 May. In neither of these cases is the point component in the location expected for the third quasar image, south of the nucleus of the primary lens galaxy G1.

c) Models Consisting of Two Point Sources (Model 3)

One possible origin of the extended nature of radio source G is that it consists of two distinct sources, one due to emission from the lens galaxy G1 itself plus a second due to the third quasar image B2. The latter would lie between the galaxy nucleus and the bright B1 image, i.e., a few tenths of an arc second south of the galaxy nucleus. One unbiased way to test this possibility is to fit two point sources to G. If one allows the position and intensity of both components to vary (Model 3), the result is (not surprisingly) roughly equal sources, separated by $0''.22$–$0''.28$, which lie along the major axes of the single Gaussians which fit the same maps (see Fig. 3). In no case is the quality of the fit the equal of that using a single Gaussian although the number of parameters is the same (compare the residuals listed in Tables 2 and 3). The total flux of the two point components is about 10% less than that in an elliptical Gaussian model, suggesting that the structure of G is not simply two point sources.

The two-point models do provide fair representations of the data, and an average over the results for the four maps shows that the northernmost of the pair of sources (GN) lies $0''.17 \pm 0''.03$ north of the optical nucleus of the galaxy G1 (combined optical and radio errors, dominated by the optical). This is illustrated clearly in Figure 3. Thus unless the optical position of G1 is badly in error, a model consisting of emission from the nucleus of the galaxy G1 plus the third image B2 does *not* fall naturally out of the model fitting to the radio source G. In addition, the southernmost of the pair of point sources (GS) lies $0''.07 \pm 0''.02$ south of the third VLBI source G′, so that this model does not lead to a convincing identification of the VLA analog of the VLBI source G′. However, GS may be used to place limits on the third quasar image B2, with the result that the flux ratio $B2/B1 < GS/B = 0.046 \pm 0.003$ for 1980 December and 0.033 ± 0.001 for 1982 May, with an overall average of 0.040 ± 0.004.

d) Models with a Point Component Located at the Third VLBI Source (Models 4 and 5)

Whether G′ is the third quasar image B2 or a source intrinsic to the galaxy G1, it must be present in the VLA map at some level. The 6 cm VLA flux of G′ is determined by its spectral index α ($F_\nu \propto \nu^{-\alpha}$) and its angular size. For spectral indices in the range $1.5 > \alpha > 0$, lower limits on the flux are 0.19–0.60 mJy; it will exceed these limits if there is radiation on an angular scale too large to have been detected by Gorenstein *et al.* A convincing demonstration that G′ is the third quasar image would be discovery in the G radio source of a point component with the position and flux discussed in §§ IV*a* and IV*c*. One way of testing this hypothesis is to let the IMFIT program decide where point sources are best accommodated in source G (Models 2 and 3, above). In neither case does a point source tend to lie at the anticipated VLA position of G′.

A second class of multiple-component model which may be fitted to G has one point source constrained to be at G′ while a second (unconstrained) model source accounts for the remainder of G. Model 4 is one example of such a possibility, where the remainder of the source is a second point source. This results in considerably larger residuals than does Model 3 (but has four rather than six free parameters) and does not yield a particularly good fit to the data. However, such a model does provide an upper limit on the VLA flux of the third VLBI component G′. The results are 1.59 ± 0.09 mJy for 1980 December and 1.32 ± 0.11 mJy for 1982 May, corresponding to VLA ratios G′/B of 0.059 ± 0.003 and 0.054 ± 0.005 respectively, with an overall average of 0.057 ± 0.003, roughly 1.8 times that anticipated if G′ is the third image of the VLBI core, and 3 times that permitted by Stockton's data in the absence of extinction. Thus the structure of G is compatible with the interpretation of the third VLBI source G′ as the third quasar image B2, although the remaining flux (intrinsic to the galaxy G1) is not well represented by a point source.

Model 5 consists of a point source constrained to be at G′ plus an unconstrained Gaussian ellipsoid. This model yields inconsistent results, the fitted fluxes for the point source being nonphysical (about -0.5 mJy) in each of the 1982 May maps, while the two 1980 December maps do not agree with each other. This model provides another set of limits on the third quasar image; $B2/B1 < 0.008 \pm 0.006$ for 1980 December and $B2/B1 < 0.007$ for 1982 May.

e) Models with Third Image Flux Predicted from the VLBI Data (*Model 6*)

The final model was a test of the consistency of the hypothesis that the third VLBI source G′ is the third quasar image. A point source with the VLA flux predicted in § IV*c* was fixed at the anticipated position and an unconstrained elliptical Gaussian fitted to the remainder of G. The flux of the point component was permitted to vary by $\pm 10\%$, and the range of resulting Gaussian components is reported in Table 3. While the fits are acceptable, there is a clear preference for point components smaller than those predicted, suggesting that if G′ is the third quasar image, the morphology of the remaining flux (intrinsic to the galaxy G1) is more complex than that of an elliptical Gaussian. While more complicated models could in principle be fitted to G, the limited data available would not permit acceptable determination of their parameters.

REFERENCES

Bourassa, R. R., and Kantowski, R. 1975, *Ap. J.*, **195**, 13.
Burke, W. L. 1981, *Ap. J.* (*Letters*), **244**, L1.
Clark, B. G. 1980, *Astr. Ap.*, **89**, 377.
Dyer, C. C., and Roeder, R. C. 1980, *Ap. J.* (*Letters*), **238**, L67.
Gorenstein, M. V., and Rogers, A. E. E. 1982, private communication.
Gorenstein, M. V., *et al.* 1980, *Bull. AAS*, **12**, 498.
Gorenstein, M. V., *et al.* 1983, *Science*, **219**, 54.
Greenfield, P. E., 1981, Ph.D. thesis, Massachusetts Institute of Technology.
Greenfield, P. E., Burke, B. F., and Roberts, D. H. 1980, *Nature*, **286**, 865.
Greenfield, P. E., Roberts, D. H., and Burke, B. F. 1980, *Science*, **208**, 495.
———. 1985, *Ap. J.*, **293**, 370.
Haschick, A. D., Moran, J. M., Reid, M. J., Davis, M., and Lilley, A. E. 1981, *Ap. J.* (*Letters*), **243**, L57.
Noble, R. G., and Walsh, D. 1980, *Nature*, **288**, 69.
Owen, F. N., Hardee, P. E., and Bignell, R. C. 1980, *Ap. J.* (*Letters*), **239**, L11.
Pauliny-Toth, I. I. K., Preuss, E., Witzel, A., Graham, D., Kellerman, K. I., and Ronnang, B. 1981, *A.J.*, **86**, 371.
Perley, R. 1982, private communication.
Pooley, G. G., Browne, I. W. A., Daintree, E. J., Moore, P. K., Noble, R. G., and Walsh, D. 1979, *Nature*, **280**, 461.
Porcas, R. W., Booth, R. S., Browne, I. W. A., Walsh, D., and Wilkinson, N. 1979, *Nature*, **282**, 385.
Porcas, R. W., Booth, R. S., Browne, I. W. A., Walsh, D., and Wilkinson, N. 1981, *Nature*, **289**, 758.
Refsdal, S. 1964, *M.N.R.A.S.*, **128**, 307.
Reid, M. J., Schmitt, J. H. M. M., Owen, F. N., Booth, R. S., Wilkinson, P. N., Shaffer, D. B., Johnston, K. J., and Hardee, P. E. 1982, *Ap. J.*, **263**, 615.
Roberts, D. H., Greenfield, P. E., and Burke, B. F. 1979, *Science*, **205**, 894.
Schwab, F. 1980, *Proc. SPIE*, **231**, 18.
———. 1981, *VLA Sci. Memorandum* (NRAO), No. **136**.
Sramek, R. A. 1982, in *Synthesis Mapping*, ed. A. R. Thompson and L. R. D'Addario (Green Bank: National Radio Astronomy Observatory, WV), p. 2–1.
Stockton, A. 1980, *Ap. J.* (*Letters*), **242**, L141.
Turland, B. D. 1975, *M.N.R.A.S.*, **170**, 281.
Walsh, D., Carswell, R. F., and Weymann, R. J. 1979, *Nature*, **279**, 381.
Weymann, R. J., Chaffee Jr., F. H., Davis, M., Carleton, N. P., Walsh, D., and Carswell, R. F. 1979, *Ap. J.* (*Letters*), **233**, L43.
Wills, B. J., and Wills, D. 1980, *Ap. J.*, **238**, 1.
Young, P., Gunn, J. E., Kristian, J., Oke, J. B., and Westphal, J. 1980, *Ap. J.*, **241**, 507.
———. 1981, *Ap. J.*, **244**, 736.

Bernard F. Burke and Jacqueline N. Hewitt: Physics Department 26-335, Massachusetts Institute of Technology, Cambridge, MA 02139

Andrea K. Dupree: Harvard-Smithsonian Center for Astrophysics, 60 Garden Street, Cambridge, MA 02138

Perry E. Greenfield: Johns Hopkins Applied Physics Lab, Laurel, MD 20707

David H. Roberts: Physics Department, Brandeis University, Waltham, MA 02254